ACS APPLIED MATERIALS & INTERFACES

Research Article

www.acsami.org

Double-Striped Metallic Patterns from PS-*b*-P4VP Nanostrand Templates

Ximin Chen, Iryna I. Perepichka,[†] and C. Geraldine Bazuin*

Département de chimie, Centre de recherche sur les matériaux auto−assemblés (CRMAA/CSACS), Université de Montréal, C.P. 6128 Succ. Centre−ville, Montréal, Quebec, Canada, H3C 3J7

Supporting Information

ABSTRACT: A new nanometallic pattern, characterized by randomly disposed double or twin one-dimensional stripes and that adds to the nanotechnology toolbox, has been obtained from a unique template possessing the nanostrand morphology. This morphology had previously been shown to form in Langmuir−Blodgett films made from a polystyrene-poly(4-vinylpyridine) (PS-P4VP) diblock copolymer blended with 3-*n*-pentadecylphenol (PDP). The nanostrand backbone is composed of PS, and it is bordered along both sides by a P4VP monolayer, visualized for the first time by high resolution atomic force microscopy. The exposed P4VP alongside the nanostrands serves as sites for depositing compounds attracted selectively to P4VP. Here, both gold ions ($HAuCl_4 \cdot 3H_2O$) and gold nanoparticles (AuNP, 12 nm in diameter, stabilized with sodium citrate) were complexed to the P4VP. Plasma treatment of the gold ions led to double stripes of monolayer metallic gold. To obtain dense deposition of AuNP in double rows, it was necessary to acidify the AuNP aqueous solution (pH 5.2 here). The achievement of the metallic double-stripe patterns also confirms the composition of the nanostrand morphology, which up to now had been deduced indirectly. The double-stripe pattern has possible applications for plasmonic lasers, energy transport, and biosensors.

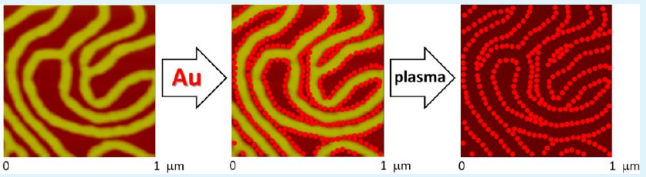

KEYWORDS: *block copolymer template, nanostrands, double stripes, 1D array, gold nanoparticles, PS-P4VP, Langmuir−Blodgett*

INTRODUCTION

The fabrication of metallic nanostructures is an effervescent area of research in view of a large variety of nanotechnological applications covering diverse domains such as catalysis,[1] optoelectronics,[2] and (bio)sensors.[3] To circumvent time-consuming, complex, and therefore costly "top-down" lithographic techniques for achieving nanoscopic structures, the spontaneous self-assembly of block copolymers has become an extensively investigated "bottom-up" alternative approach, including in combination with greater length-scale lithographic methods.[4−15] Block copolymer self-assembly relies on the phase separation between dissimilar blocks, which is controlled by the block composition (and hence the Flory−Huggins interaction parameter χ), the total molecular weight, and the block volume fractions. Further control can be achieved by the addition of block selective materials (small molecules, homopolymer, inorganic substances, etc.) that modify the relative phase volumes and interaction parameters, also known as supramolecular control.[16−21] Unique structures can be achieved in thin and ultrathin films due to the importance of interfacial interactions, typically with air and substrate (solid or liquid), and of film thickness relative to the natural periodicity of the block copolymer.[5,8−10,13,22] Reproducible kinetic control is also used extensively to control the self-assembly outcomes, influenced, for example, by the choice of solvent used for film preparation or by solvent annealing.[17−19,23−27]

Many nanotechnological applications require the patterning of metals such as gold into specific nanostructures.[4−15] These structures can be conveniently prepared (a) through the self-assembly of block copolymers preassociated with the metal nanoparticles or their precursors in solution[28−34] or (b) by deposition of the nanoparticles or their precursors on preassembled block copolymer (or other molecular) patterns acting as nanotemplates.[17−19,31,35−39] The most usual patterns obtained with block copolymer thin films are (a) nanodots, obtained with block copolymer films that self-assemble in the form of spherical micelles or vertical cylinders (rods), and (b) nanostrands (stripes, wires), obtained with block copolymer films that self-assemble in the form of horizontal cylinders or side-on lamellae.

Here, we show that gold can be patterned in the form of randomly disposed double (or twin) stripes of atomic monolayers or of rows of nanoparticles, a new type of pattern that adds to the nanotechnology toolbox, with possible applications in plasmonic lasers, energy transport, and biosensors.[40−42] This achievement relies on using a template having a loosely packed nanostrand pattern obtained from Langmuir−Blodgett (LB) monolayers of polystyrene-*b*-poly(4-vinylpyridine) (PS-P4VP) blended with 3-*n*-pentadecylphenol (PDP) that hydrogen bonds to P4VP, as described previously.[43,44] The conditions required for the nanostrand morphology to form at the air/water interface from this system

Received: September 15, 2014
Accepted: September 26, 2014
Published: September 26, 2014

are the use of block copolymers with moderate hydrophilic content (9−19 mol % P4VP for equimolar PDP relative to the 4VP repeat unit[45]) and relatively high spreading solution concentration. Typically, the nanostrands do not cover the entire surface but are separated from one another to a significant extent. They are assumed to be composed of a PS backbone, raised with respect to the water surface to minimize repulsive interactions, and a hydrophilic P4VP monolayer that lies beneath and along both sides of the PS backbone, as illustrated in Figure 1. It is anticipated that molecules that bond

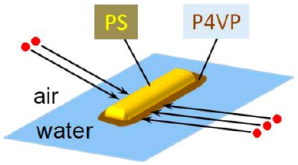

Figure 1. Schematic representation of a short nanostrand segment, illustrating its composition; the red dots represent gold that is expected to be deposited on the exposed P4VP alongside the PS backbone, as indicated by the arrows.

or complex to P4VP will be selectively located on the narrow P4VP stripes exposed alongside the PS backbone. The strategy will be shown to be successful for templating gold ions, which can then be converted to double stripes of gold monolayer after plasma treatment, as well as for templating gold nanoparticles (AuNPs) directly.

Furthermore, the success of the selective deposition in the form of double stripes provides clear evidence that P4VP is indeed exposed along the periphery of the nanostrands and well phase-separated from the PS backbone. Previously, this was concluded indirectly from atomic force microscopy (AFM) and other observations for various amphiphilic block copolymers,[46−51] and from the air/water interface characteristics assuming that, during LB monolayer deposition, the structure on the water surface is transferred to polar solid substrates with little or no perturbation.[44,45] In other words, given the polarity of the water surface and block copolymer composition, it was logical to attribute the several nanometer-high backbone seen in the AFM topographic images to hydrophobic chain aggregation and to posit that the hydrophilic block was spread as a monolayer beneath and alongside the backbone, thereby preventing lateral coalescence of the hydrophobic backbones. However, no direct proof of the composition of the high and low regions has been provided until now. This paper will, in addition, show high-resolution AFM images in which the P4VP monolayer itself is visualized for the first time. It will end with a brief discussion concerning possible applications.

EXPERIMENTAL SECTION

Materials. Polystyrene-*b*-poly(4-vinylpyridine) (PS-P4VP) with M_n(PS) = 40 000 g/mol, M_n(P4VP) = 5600 g/mol (384 S repeat units, 53 VP repeat units, 12 mol % VP content), and M_w/M_n = 1.09, was obtained from Polymer Source (Dorval, QC, Canada) and used as received. 3-*n*-Pentadecylphenol (PDP) (Sigma-Aldrich, 90%) was recrystallized twice from hexane (0.3 g/mL) before use. Chloroform ($CHCl_3$, HPLC grade, ≥99.8%) and 1,1,2,2-tetrachloroethane ($C_2H_2Cl_4$, GC grade, ≥98.0%) from Fluka were used as spreading solvents, following ref 44. All other chemicals were used as received: hydrogen tetrachloroaurate trihydrate ($HAuCl_4{\cdot}3H_2O$, 99.9%) from Strem Chemicals, trisodium citrate dihydrate (ACS reagent grade, ≥99.0%) from Sigma-Aldrich, and methanol (MeOH, 99.9%) from VWR. Ultrapure water (18.2 MΩ cm) was obtained by purification of distilled water with a Millipore Milli-Q Gradient system. Muscovite ruby mica (ASTM grade 2, B&M Mica, Flushing, NY, U.S.A.) was cleaved immediately before its immersion into the subphase.

Langmuir−Blodgett (LB) Monolayer Films (LB Nanostrand Templates). Detailed conditions for the preparation of LB films with a nanostrand morphology have been described by us previously.[44] Briefly, PS-P4VP was dissolved in $CHCl_3$ (for loosely packed or "loose" nanostrands) or $C_2H_2Cl_4$ (for densely packed or "dense" nanostrands) at solution concentrations of 2 mg/mL, and PDP was added at a 4VP/PDP molar ratio of 1:1.2. The solutions were left to stir overnight at room temperature in sealed volumetric flasks. A computer-controlled KSV 3000 Langmuir−Blodgett system with a platinum Wilhelmy plate sensing device (KSV Instruments, Helsinki, Finland) was used for monolayer deposition. The subphase temperature in the trough (150 × 518 mm) was maintained at 20−21 °C for $CHCl_3$ solutions and 10−11 °C for $C_2H_2Cl_4$ solutions using a refrigerated circulator (Isotemp 3016, Fisher Scientific). Freshly cleaved mica substrates (size ranging from 1 × 2.5 to 2 × 3 cm^2) were immersed into the subphase at the center of the Langmuir trough. Using a Hamilton microliter syringe, 50 (for $CHCl_3$) or 70 (for $C_2H_2Cl_4$) μL of solution were spread dropwise on the water surface in a checkerboard pattern, followed by a pause of 30 (for $CHCl_3$) or 50−60 (for $C_2H_2Cl_4$) min for solvent evaporation. Barriers were then symmetrically compressed at a speed of 10 mm/min (15 cm^2/min) to a surface pressure of 5 (for $CHCl_3$) or 11 (for $C_2H_2Cl_4$) mN/m (the higher pressure for $C_2H_2Cl_4$ improved substrate coverage), followed by a 25−30 min wait for barrier stabilization at this pressure. The monolayer films were deposited on the mica substrates by vertically withdrawing them out of the subphase at a controlled speed of 5 mm/min. Transfer ratios were 1.0 ± 0.2. The deposited films were dried in a clean box overnight at room temperature before AFM imaging or further film treatment.

LB Film Treatment. If not specified otherwise, the LB monolayer templates were used as prepared. If PDP removal prior to gold deposition is mentioned, the film-covered substrate was immersed in MeOH for a specified time. In some cases, the LB film was UV-irradiated for 2 h, using a UVC-14 UV lamp (Ultra-Lum) with a 4-W output at 254 nm (lamp−sample distance, 5 cm).

Gold Ion Deposition and Plasma Treatment. $HAuCl_4{\cdot}3H_2O$ was dissolved in MeOH or in ultrapure water to the desired concentration (typically, 39 mg in 10 mL). The LB templates were immersed in the solution for the desired time (typically 30 min), then thoroughly rinsed with MeOH or ultrapure water and dried under a nitrogen stream. To reduce the gold ions to atomic gold and remove the exposed polymer,[28−30] the samples were placed in an oxygen plasma chamber (Harrick Scientific PDC-32G plasma cleaner/sterilizer), and treated for 1.5−2 min at a medium RF level and an O_2 flow rate of 13.4 mL/min controlled by a Praxair PRS FM4301-1 15 cm flow meter. The samples were analyzed within about 30 min after plasma treatment, since aggregates appeared over time (see Supporting Information Figure SI-1).

AuNP Synthesis and Deposition. Citrate-stabilized AuNPs were synthesized using the Turkevich-Frens method.[52,53] This consisted of dissolving 10 mg (0.025 mmol) of $HAuCl_4{\cdot}3H_2O$ in 50 mL of ultrapure water, heating to reflux, then adding all at once, during vigorous stirring at reflux, a trisodium citrate aqueous solution (typically, about 30 mg of trisodium citrate in 5 mL ultrapure water, giving a Au(III)/citrate molar ratio of 1:4). The solution was observed to gradually change color from light yellow to colorless to light gray to purple and finally to wine red (completed within about 5 min), indicating AuNP formation, after which stirring at reflux was continued for another 10 min, then the solution was cooled to room temperature. It was stored at 4 °C protected from light, and used within a few days.

Formation of AuNPs was confirmed by UV−visible spectroscopy (Supporting Information Figure SI-2), which shows a plasmon absorption peak with a maximum at about 520 nm. A representative transmission electron microscopy image (Supporting Information Figure SI-3) indicates that the AuNPs were spherical and quite monodisperse, with an average diameter of 12 ± 1 nm. This diameter was confirmed by AFM, as indicated in the Results section.

The nanostrand templates on mica were immersed for 60 min in AuNP solutions as prepared (pH in the range 5.8−6.2) or acidified by addition of HCl to attain a pH of 5.2, then rinsed for about 1 min with ultrapure water, and dried under nitrogen flow. The samples were then subjected to oxygen plasma as described above to remove the exposed polymer.

Atomic Force Microscopy (AFM). AFM images, except for those in Figure 3, were obtained in light tapping mode with a Multimode microscope and a Nanoscope III controller (Digital Instruments), operated under ambient atmosphere, using Nanoworld or AppNano tips (Nanoworld Innovative Technologies, Arrows NCR model, spring constant 42 N/m, oscillation frequency 285 kHz, tip radius ≤ 10 nm; AppNano, ACTA model; spring constant 40 N/m, oscillation frequency 300 kHz, tip radius ≤ 6 nm). Geometric parameters reported are averages based on measurements obtained from several images per film. The AFM images in Figure 3 were obtained with a SmartSPM (AIST-NT Inc., Novato, CA, U.S.A.) in semicontact mode under ambient conditions without acoustic and vibration protection using silicon probes (NanoWorld, Arrow NCR, force constant 42 mN/m, tip radius < 10 nm).

Time-of-Flight Secondary Ion Mass Spectrometry (TOF-SIMS). A plasma-treated substrate was analyzed by TOF-SIMS using a TOF-SIMS IV instrument (ION-TOF, GmbH, Münster, Germany) working at an operating pressure of about 5×10^{-9} Torr. Samples were bombarded by Bi primary ions at an energy level of 25 keV in bunch mode, with the gun operating at a 0.5 pA pulsed ion current over a frame area of 40×40 μm^2 for a dosage below the threshold level of 1×10^{13} ions/cm^2 for static SIMS. Secondary ions were detected with a reflection time-of-flight analyzer, a multichannel plate (MCPs), and a time-to-digital converter (TDC). Measurements were taken with an acquisition time of 100 s at a TDC time resolution of 200 ps. The maximum mass resolution, $R = m/\Delta m$, was ≥8000 on $^{29}Si^+$, where m is the target ion mass and Δm is the resolved mass difference at the peak half-width. Effective charge compensation was obtained using the electron flood gun. The m/z scale was calibrated using the signals of C, CH, C_2, C_2H, etc. Integration of the signals was performed using a Poisson correction.

X-ray Photoelectron Spectroscopy (XPS). The presence of reduced gold on a plasma-treated substrate was determined by XPS using a VG Escalab 3 MKII spectrometer (Thermo Scientific). Electrons were excited using nonmonochromated Mg K_α radiation at 1253.6 eV, with an experimentally determined spectral resolution of 0.7 eV and a standard error of <0.1 eV. The pressure in the analysis chamber was maintained at 10^{-9} Torr. Energy calibration was carried out by placing the hydrocarbon peak in the C 1s spectrum at 285.0 eV. The samples were analyzed at an angle of 30° with respect to the analyzer, which translates to an analyzed depth of approximately 2−3 nm.

RESULTS AND DISCUSSION

High Resolution AFM Imaging of the Nanostrands. A typical AFM topographical image of the nanostrand morphology obtained by the LB transfer of PS-P4VP/PDP (12 mol % P4VP, equimolar 4VP/PDP) to a mica substrate, along with section profiles, is shown in Figure 2. In accordance with what was reported previously,[44] the average dimensions of the nanostrands are 6−7 nm in height and 60 ± 5 nm in width, with a center-to-center distance of closest approach of about 80 nm. As stated above and shown in Figure 1, the nanostrand backbone is assigned to hydrophobic PS, and it is presumed that hydrophilic P4VP lies as a monolayer adsorbed to the water surface beneath and alongside the PS. PDP is associated with P4VP by hydrogen bonding (possibly with a small fraction associated with PS[54,55]), thereby causing this block to take on an extended conformation. Consistent with this, the closest distance between nanostrands (15−25 nm) compares well with one to two fully extended P4VP chain lengths (13−26 nm).

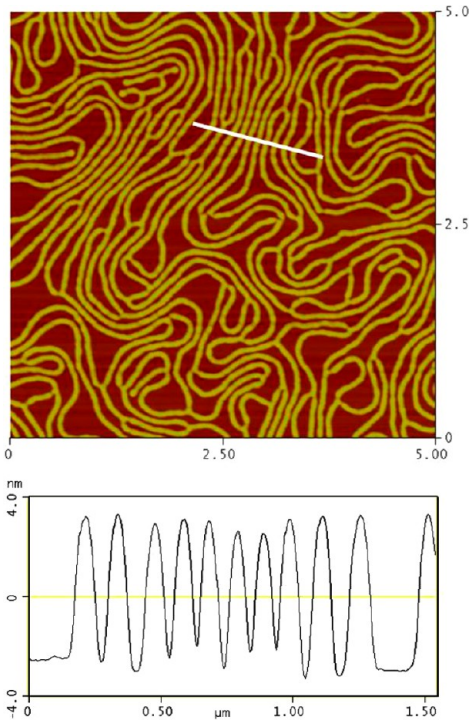

Figure 2. AFM topographic image (5×5 μm^2) and a section profile (along the white line in the top image) of a PS-P4VP/PDP LB film transferred at a surface pressure of 5 mN/m to a mica substrate.

Since the P4VP segments cannot cover more than two fully extended lengths (one length from each neighboring nanostrand), spaces between nanostrands that are larger than about 25 nm must be bare substrate. However, no height difference between the P4VP/PDP monolayer alongside the strands and the bare substrate can be detected in usual AFM topographic images, due to insufficient vertical resolution. This also implies that the PDP alkyl chains lie in a prone position relative to the surface, consistent with results for low surface-pressure LB films of PS-P4VP/PDP having a nanodot morphology.[56]

Recent developments in AFM imaging has led to greater resolution capabilities that allow visualization of the hydrophilic monolayer for the first time to our knowledge. This is shown in Figure 3, where the monolayer is apparent as purple-colored areas along both sides of the nanostrands, with black areas observed between them in many places. The section profiles (Figure 3b, d) show a low-lying plateau-like region (indicated by stars) alongside each peak (PS backbone) with a still lower area (bare substrate) centered between the two peaks. The plateau width is about 10−15 nm, consistent with the length of extended P4VP block strands, and its height is about 0.6 nm relative to the substrate, consistent with the monolayer form of P4VP and prone PDP.

In what follows, it will be demonstrated that the P4VP monolayer alongside the strands allows for selective deposition of metals, thereby lending further proof of its presence and availability at those locations. The nanostrands thus provide a unique template for obtaining twin metal stripes. This will be shown (a) by adsorption of gold ions followed by their conversion into metallic gold, resulting in double stripes of gold monolayer, and (b) by the deposition of gold nanoparticles patterned in the form of double rows.

Twin Gold Monolayer Stripes from Gold Ions. By immersing the nanostrand template in a $HAuCl_4$ solution,

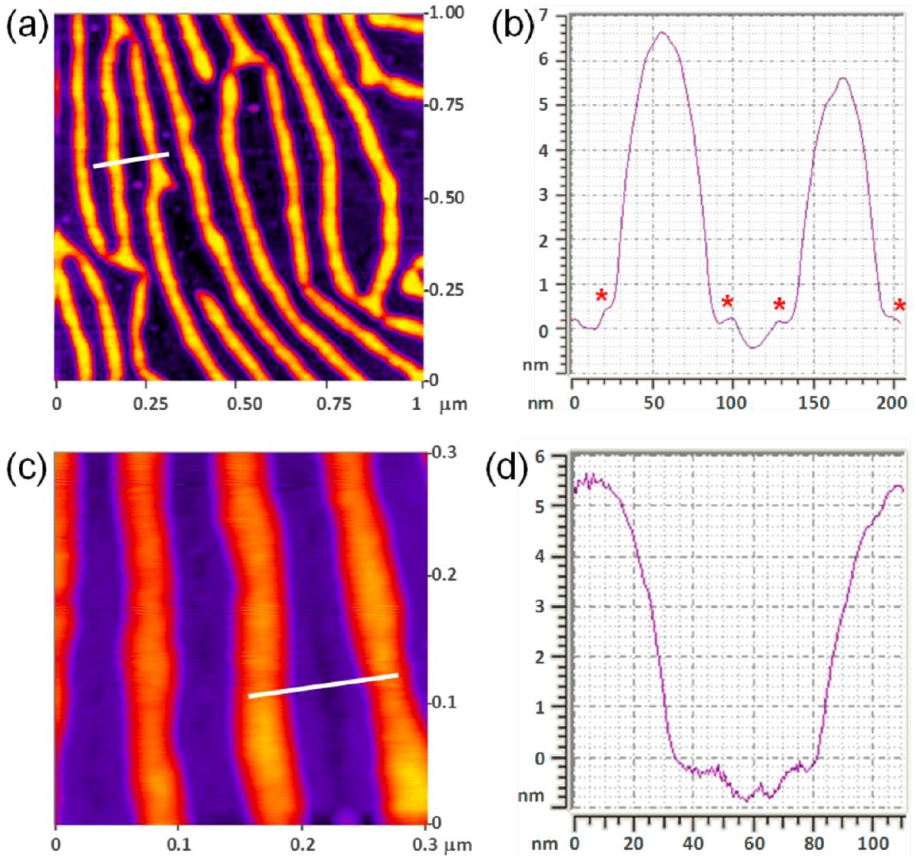

Figure 3. AFM topographic images [(a) 1 × 1 μm^2; (c) 300 × 300 nm^2] and section profiles (b, d), along the white lines in images a and c, of the PS-P4VP/PDP LB film transferred at a surface pressure of 5 mN/m.

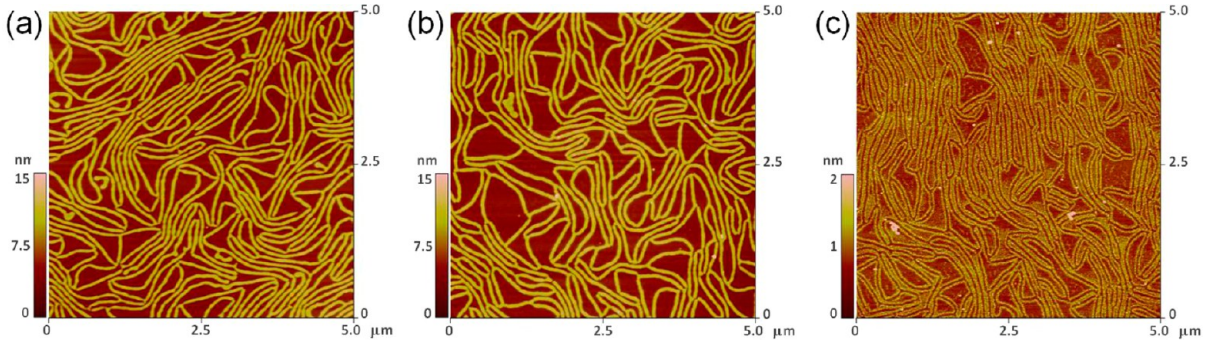

Figure 4. AFM topographic images (5 × 5 μm^2) of (a) a PS-P4VP nanostrand template obtained by the LB technique, (b) Au^{3+}-loaded PS-P4VP nanostrands, and (c) double nanostripes of Au^0 monolayer after plasma treatment.

exposed P4VP is protonated by $HAuCl_4$ in an acid−base reaction and thereby can electrostatically bind $AuCl_4^-$ ions.[57] Oxygen plasma can then be used to reduce Au^{3+} to Au^0 (or complete the reduction, if already reduced in part by exposure to ambient atmosphere[9]), which occurs via the intermediate formation of the unstable gold oxide, Au_2O_3, from which metallic gold is obtained as a decomposition product.[58] Figure 4 shows a sequence of AFM topographical images, starting from (a) the original nanostrand template (after UV irradiation for 2 h to cross-link the film[59,60]) to (b) its appearance after immersion into a $HAuCl_4$ solution (10 mM in methanol) for 30 min and, finally, (c) after plasma treatment. The operations prior to the plasma treatment do not perturb the template, and the average height and width of the nanostrands remain constant. Au^{3+} loading on the nanostrands cannot be seen in Figure 4b, due to the very small size of the ions. The plasma treatment, which removes the exposed polymer (i.e., the nanostrand backbones) in addition to converting gold ions to metallic gold, leaves clear outlines of the original nanostrands in the form of two very thin stripes that are presumably composed of metallic gold (Figure 4c). This is particularly obvious wherever isolated nanostrand segments had crossed bare substrate. The double stripes are separated by about 60 nm, which is comparable to the original width of the nanostrands and consistent with the supposition that gold ion complexation to the P4VP lying alongside the nanostrands took place. The presence of gold on the plasma-treated substrates was confirmed by TOF-SIMS, which gave a negative polarity peak at 196.91 uma, very close to the expected value of 196.96656 uma for Au^-. Its form as atomic gold (Au^0) was supported by

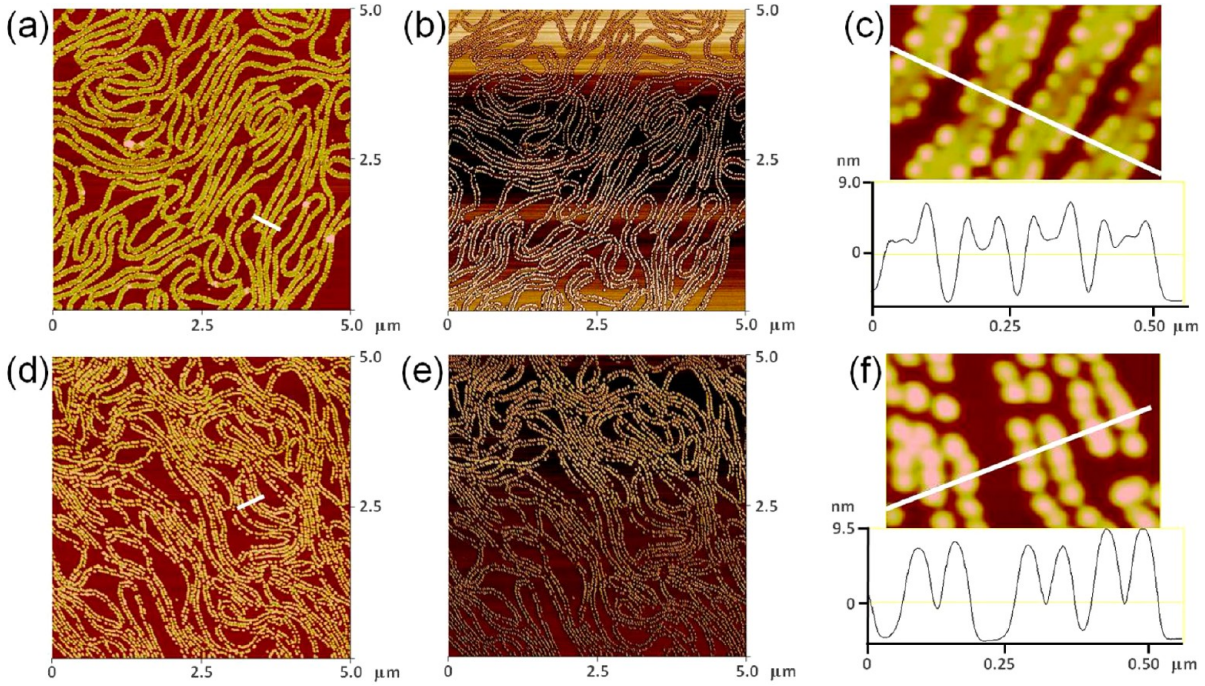

Figure 5. AFM images ($5 \times 5\ \mu m^2$) of AuNPs (top) adsorbed to a loose nanostrand template and (bottom) after plasma treatment removing the exposed polymer [(a, d) height images; (b, e) phase images; (c, f) expanded regions around the white lines shown in images a and d, respectively, along with corresponding section profiles].

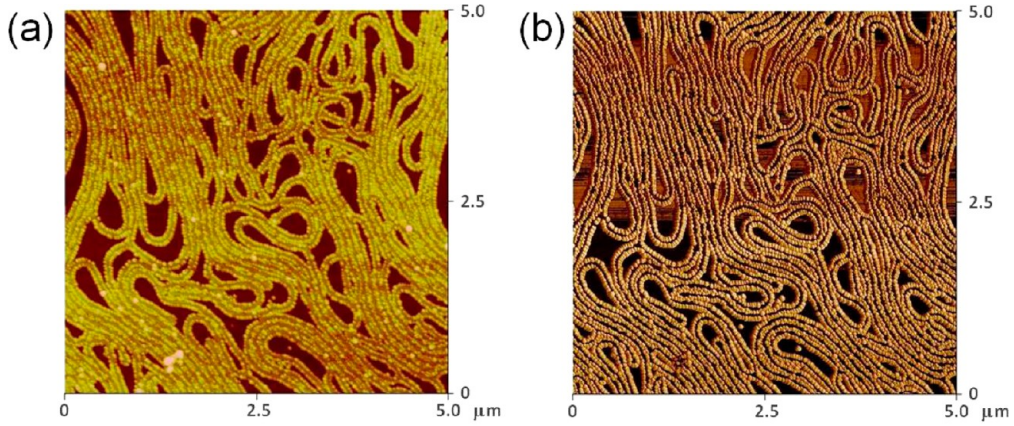

Figure 6. AFM images ($5 \times 5\ \mu m^2$) of AuNPs adsorbed to a dense nanostrand template (no plasma treatment was applied): (a) height image (z-scale: 20 nm); (b) phase image.

XPS, which showed peaks at 84 and 88 eV, corresponding to Au $4f_{7/2}$ and $4f_{5/2}$, respectively, and peaks at 335 and 353 eV, corresponding to Au $4d_{5/2}$ and $4d_{3/2}$, respectively. The height of the stripes is 0.3−0.6 nm (noting that the z-scale in Figure 4c is 2 nm compared to 15 nm in Figure 4a, b). Since gold atoms have a diameter of 0.29 nm (and considering that P4VP monolayer may still lie beneath the gold stripes due to being shielded from the plasma by the latter), it can be concluded that the stripes are composed mainly of an atomic monolayer of metallic gold.

The sequence shown in Figure 4 was repeated with essentially the same results for a range of experimental conditions: notably, by varying the $HAuCl_4$ concentration in solution (tested for 5 to 20 mM with MeOH solutions), by increasing the template immersion time in solution (tested up to 2 h for 10 and 20 mM $HAuCl_4$ solutions in MeOH), and by using aqueous instead of methanolic gold ion solutions. Furthermore, although UV cross-linking was generally used to preclude possible template instability (such as washing off or reorganization),[59,60] it was in fact found to be unnecessary. The possibility that H-bonded PDP could block access of $HAuCl_4^-$ to P4VP was also considered, and thus, initially, the templates were immersed in MeOH for 1−10 min (as in Figure 4a) before UV cross-linking. Further tests showed that this also was unnecessary for both methanolic and aqueous $HAuCl_4$ solutions; for the former, in which PDP is soluble, it is removed in any case, whereas possible slight solubility in aqueous solution may also be enough to enable its removal (or displacement) there. It was found, however, that the gold monolayer stripes are unstable over time, with a tendency to aggregate or fuse into larger particles, as shown by comparing AFM images taken within 5 to 30 min after plasma treatment with ones taken about 2 days later (Supporting Information Figure SI-1; times between 30 min and 40 h were not

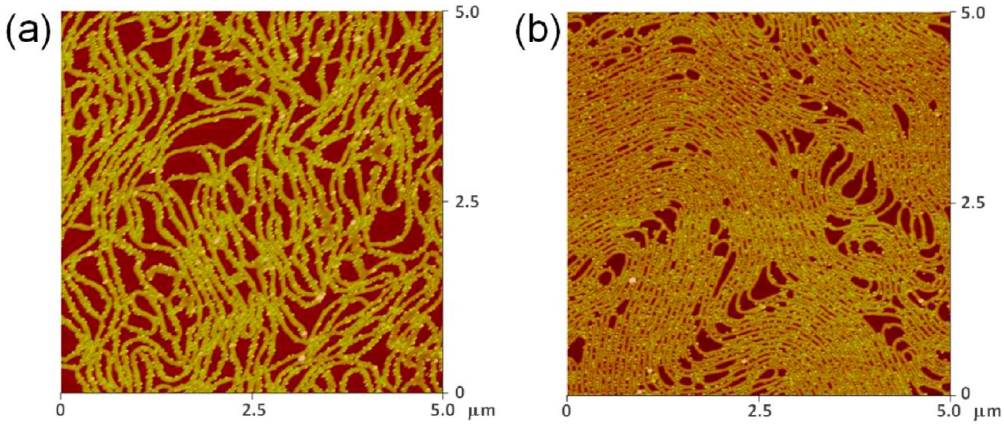

Figure 7. AFM topographic images (5 × 5 μm^2; z-scale 20 nm) of AuNPs adsorbed to (a) a loose and (b) a dense nanostrand template using an as-prepared AuNP solution with no added HCl (pH 6; no plasma treatment applied).

investigated). Nevertheless, the window of stability, which may extend to several hours, might be sufficient for subsequent developmental steps for certain applications.

Deposition of Gold Nanoparticles in Double Rows. Citrate-stabilized AuNPs are known to adsorb to P4VP and P2VP, selectively, in the case of block copolymers and blends based on these polymers.[35,61,62] To apply this in the present case, LB nanostrand templates were prepared using both chloroform and 1,1,2,2-tetrachloroethane ($C_2H_2Cl_4$) as spreading solvents. In comparison with relatively loose nanostrands obtained when using $CHCl_3$, $C_2H_2Cl_4$ leads to much denser and more mutually aligned nanostrand packing, where the raised PS backbones are separated by low-lying P4VP monolayer with little or no bare substrate exposed between the nanostrands, but with larger regions of bare substrate exposed within the overall pattern or film.[44] In what follows, the two types of nanostrand templates will be referred to as "loose" and "dense", respectively.

For both types of template, it was found that, for reproducibly high-density AuNP deposition, the AuNP solution must be acidified (see below), which was done to a pH of 5.2. The AFM images in Figures 5 and 6 for loose and dense templates, respectively, show that adsorption of AuNPs from acidified solution takes place selectively on the P4VP stripes, particularly apparent for isolated strand segments. Clearly, the AuNPs are packed densely in parallel rows on either side of the PS nanostrand backbones. The section profile in Figure 5c shows that the height of the nanostrands is unchanged from before deposition (7 ± 1 nm), whereas the height of the AuNPs is 12 ± 2 nm. The AuNPs remain densely packed in two parallel rows following plasma treatment (Figure 5), which removes the exposed polymer (PS backbone) between the double rows of AuNPs. The absence of the backbone is shown by the section profile in Figure 5f, which also indicates that the height of the AuNPs is unchanged and that the average center-to-center distance between the double rows is about 65 nm. Again, it was noted that prior rinsing of the templates in MeOH to remove PDP is unnecessary, as above for Au^{3+} deposition. On the other hand, prior exposure of the templates to UV cross-linking was found to inhibit AuNP deposition, in contrast to the case for Au^{3+} deposition. The patterns appear to be stable over time, with no fusion or aggregation observed.

If as-prepared AuNP solutions, for which the pH is around 6, are used, AuNP deposition is generally much sparser (tested for immersion times up to 2 h). This is shown, for example, in Figure 7 for both loose and dense templates, prepared in parallel with the samples shown in Figures 5 and 6. For the loose template, the relatively isolated AuNPs are visible as protrusions alongside the nanostrands. For the dense template, they appear mainly as particles located in the low-lying stripes between the nanostrand backbones. The relative sparseness of the AuNP deposition concords with ref 61, where it was found that AuNPs deposited on a P4VP homopolymer film tended to remain well separated even after several hours of soaking time; this was attributed to repulsive interactions among the negatively charged AuNPs. In contrast, the critical role of the pH can be attributed to electrostatic interactions that attract the negative citrate ion-protected AuNPs to P4VP that is positively charged by protonation.[63] Although the fraction of 4VP units actually protonated during soaking is unknown due to their location on the substrate surface rather than in solution, it may be noted that in aqueous solution at the pH used (5.2) the 4VP would be about 50% protonated given that the pK_a of the conjugate acid of pyridine is 5.25.

An interest of these nanostructures is that there is a preferred distance determined by the separation of the paired strands. This distance, on the order of a few tens of nanometers, can be tuned by the block copolymer molecular weight and block weight fractions (within the limits producing the nanostrand morphology[45]) as well as, to some extent, the nanoparticle size. This, coupled with the ability to modulate the nearest interparticle distance along the strands by nanoparticle diameter (and potential tweaking of properties by the adsorption density), should add to the current interest in linear or 1D plasmonic arrays.[40−42] These types of arrays have received much less attention to date compared to 2D and 3D arrays of often isolated NPs, yet they display unique optical (e.g., surface plasmon resonance and waveguiding) and electromagnetic properties, with potential applications in laser plasmonics, energy transport, and (bio)sensors.[40−42] As one example, strand pairs might serve as optical connectors for energy transport devices, where light entering one strand is transmitted to the output of both strands via plasmonic coupling.

CONCLUSIONS

It had been shown previously that a nanostrand morphology, presumably composed of a hydrophobic backbone lying atop a hydrophilic monolayer strip, can be obtained from a PS-P4VP diblock copolymer mixed with equimolar PDP, using the

Langmuir–Blodgett technique. Here, we have demonstrated that both gold ions and gold nanoparticles can be deposited selectively on the exposed P4VP alongside the PS backbone of the nanostrands, leading to twinned one-dimensional patterns of gold. Such patterns, particularly of AuNPs, may have potential applications for, for example, plasmonic biosensors. This strategy for obtaining double-stripe patterns should be applicable to any compound with selective affinity for P4VP. Furthermore, the selective deposition confirms the composition of the nanostrand structure, which up to now had been deduced indirectly. In addition, high resolution AFM imaging permitted visualization of the P4VP monolayer along the strands.

■ ASSOCIATED CONTENT

Ⓢ Supporting Information

AFM height images of Au^0 monolayers at different times after plasma treatment, UV–visible spectrum and transmission electron micrograph of the AuNPs synthesized. This material is available free of charge via the Internet at http://pubs.acs.org.

■ AUTHOR INFORMATION

Corresponding Author

*Email: geraldine.bazuin@umontreal.ca.

Present Address

†Polymer Source Inc., 124 Avro Street, Dorval, QC H9P 2X8, Canada.

Notes

The authors declare no competing financial interest.

■ ACKNOWLEDGMENTS

The financial support of NSERC (Canada) and FQRNT (Québec) is gratefully acknowledged. The authors thank Fedor Kraev (UC Davis, U.S.A.) for his contribution to the high-resolution AFM imaging and Prof. Jean-François Masson in our department for discussion regarding potential applications.

■ REFERENCES

(1) Hvolbæk, B.; Janssens, T. V.; Clausen, B. S.; Falsig, H.; Christensen, C. H.; Nørskov, J. K. Catalytic Activity of Au Nanoparticles. *Nano Today* **2007**, *2*, 14–18.

(2) Haberkorn, N.; Lechmann, M. C.; Sohn, B. H.; Char, K.; Gutmann, J. S.; Theato, P. Templated Organic and Hybrid Materials for Optoelectronic Applications. *Macromol. Rapid Commun.* **2009**, *30*, 1146–1166.

(3) Bolduc, O. R.; Masson, J.-F. Advances in Surface Plasmon Resonance Sensing with Nanoparticles and Thin Films: Nanomaterials, Surface Chemistry, and Hybrid Plasmonic Techniques. *Anal. Chem.* **2011**, *83*, 8057–8062.

(4) Hamley, I. W. Nanotechnology with Soft Materials. *Angew. Chem., Int. Ed.* **2003**, *42*, 1692–1712.

(5) Hamley, I. W. Ordering in Thin Films of Block Copolymers: Fundamentals to Potential Applications. *Prog. Polym. Sci.* **2009**, *34*, 1161–1210.

(6) Park, C.; Yoon, J.; Thomas, E. L. Enabling Nanotechnology with Self Assembled Block Copolymer Patterns. *Polymer* **2003**, *44*, 6725–6760.

(7) Krishnamoorthy, S.; Hinderling, C.; Heinzelmann, H. Nanoscale Patterning with Block Copolymers. *Mater. Today* **2006**, *9*, 40–47.

(8) Segalman, R. A. Patterning with Block Copolymer Thin Films. *Mater. Sci. Eng.* **2005**, *R48*, 191–226.

(9) Li, M.; Coenjarts, C. A.; Ober, C. K. Patternable Block Copolymers. *Adv. Polym. Sci.* **2005**, *190*, 183–226.

(10) Darling, S. B. Directing the Self-Assembly of Block Copolymers. *Prog. Polym. Sci.* **2007**, *32*, 1152–1204.

(11) Olson, D. A.; Chen, L.; Hillmyer, M. A. Templating Nanoporous Polymers with Ordered Block Copolymers. *Chem. Mater.* **2008**, *20*, 869–890.

(12) Kim, H.-C.; Park, S.-M.; Hinsberg, W. D. Block Copolymer Based Nanostructures: Materials, Processes, and Applications to Electronics. *Chem. Rev.* **2010**, *110*, 146–177.

(13) Marencic, A. P.; Register, R. A. Controlling Order in Block Copolymer Thin Films for Nanopatterning Applications. *Annu. Rev. Chem. Biomol. Eng.* **2010**, *1*, 277–297.

(14) Kim, J. K.; Yang, S. Y.; Lee, Y. M.; Kim, Y. S. Functional Nanomaterials Based on Block Copolymer Self-Assembly. *Prog. Polym. Sci.* **2010**, *35*, 1325–1349.

(15) Stoykovich, M. P.; Kang, H.; Daoulas, K. Ch.; Liu, G.; Liu, C.-C.; de Pablo, J. J.; Müller, M.; Nealey, P. F. Directed Self-Assembly of Block Copolymers for Nanolithography: Fabrication of Isolated Features and Essential Integrated Circuit Geometries. *ACS Nano* **2007**, *1*, 168–175.

(16) van Zoelen, W.; ten Brinke, G. Thin Films of Complexed Block Copolymers. *Soft Matter* **2009**, *5*, 1568–1582.

(17) Nandan, B.; Gowd, E. B.; Bigall, N. C.; Eychmüller, A.; Formanek, P.; Simon, P.; Stamm, M. Arrays of Inorganic Nanodots and Nanowires Using Nanotemplates Based on Switchable Block Copolymer Supramolecular Assemblies. *Adv. Funct. Mater.* **2009**, *19*, 2805–2811.

(18) Böhme, M.; Kuila, B.; Schlörb, H.; Nandan, B.; Stamm, M. Thin Films of Block Copolymer Supramolecular Assemblies: Microphase Separation and Nanofabrication. *Phys. Status Solidi B* **2010**, *247*, 2458–2469.

(19) Gowd, E. B.; Nandan, B.; Bigall, N. C.; Eychmüller, A.; Formanek, P.; Stamm, M. Hexagonally Ordered Arrays of Metallic Nanodots from Thin Films of Functional Block Copolymers. *Polymer* **2010**, *51*, 2661–2667.

(20) Roland, S.; Prud'homme, R. E.; Bazuin, C. G. Morphology, Thickness, and Composition Evolution in Supramolecular Block Copolymer Films over a Wide Range of Dip-Coating Rates. *ACS Macro Lett.* **2012**, *1*, 973–976.

(21) Lin, Y.; Böker, A.; He, J.; Sill, K.; Xiang, H.; Abetz, C.; Li, X.; Wang, J.; Emrick, T.; Long, S.; Wang, Q.; Balazs, A.; Russell, T. P. Self-Directed Self-Assembly of Nanoparticle/Copolymer Mixtures. *Nature* **2005**, *434*, 55–59.

(22) Fasolka, M. J.; Mayes, A. M. Block Copolymer Thin Films: Physics and Applications. *Annu. Rev. Mater. Res.* **2001**, *31*, 323–355.

(23) Park, S.; Wang, J.-Y.; Kim, B.; Chen, W.; Russell, T. P. Solvent-Induced Transition from Micelles in Solution to Cylindrical Microdomains in Diblock Copolymer Thin Films. *Macromolecules* **2007**, *40*, 9059–9063.

(24) Paik, M. Y.; Bosworth, J. K.; Smilges, D.-M.; Schwartz, E. L.; Andre, X.; Ober, C. K. Reversible Morphology Control in Block Copolymer Films via Solvent Vapor Processing: An In Situ GISAXS Study. *Macromolecules* **2010**, *43*, 4253–4260.

(25) Phillip, W. A.; Hillmyer, M. A.; Cussler, E. L. Cylinder Orientation Mechanism in Block Copolymer Thin Films Upon Solvent Evaporation. *Macromolecules* **2010**, *43*, 7763–7770.

(26) Huang, W.-H.; Chen, P.-Y.; Tung, S.-H. Effects of Annealing Solvents on the Morphology of Block Copolymer-Based Supramolecular Thin Films. *Macromolecules* **2012**, *45*, 1562–1569.

(27) Sinturel, C.; Vayer, M.; Morris, M.; Hillmyer, M. A. Solvent Vapor Annealing of Block Polymer Thin Films. *Macromolecules* **2013**, *46*, 5399–5415.

(28) Spatz, J. P.; Mössmer, S.; Hartmann, C.; Möller, M.; Herzog, T.; Krieger, M.; Boyen, H.-G.; Ziemann, P.; Kabius, B. Ordered Deposition of Inorganic Clusters from Micellar Block Copolymer Films. *Langmuir* **2000**, *16*, 407–415.

(29) Kästle, G.; Boyen, H.-G.; Weigl, F.; Lengl, G.; Herzog, T.; Ziemann, P.; Riethmüller, S.; Mayer, O.; Hartmann, C.; Spatz, J. P.; et al. Micellar Nanoreactors—Preparation and Characterization of

Hexagonally Ordered Arrays of Metallic Nanodots. *Adv. Funct. Mater.* **2003**, *13*, 853−861.
(30) Lohmueller, T.; Bock, E.; Spatz, J. P. Synthesis of Quasi-Hexagonal Ordered Arrays of Metallic Nanoparticles with Tuneable Particle Size. *Adv. Mater.* **2008**, *20*, 2297−2302.
(31) Aizawa, M.; Buriak, J. M. Block Copolymer Templated Chemistry for the Formation of Metallic Nanoparticle Arrays on Semiconductor Surfaces. *Chem. Mater.* **2007**, *19*, 5090−5101.
(32) Li, Q.; He, J.; Glogowski, E.; Li, X.; Wang, J.; Emrick, T.; Russell, T. P. Responsive Assemblies: Gold Nanoparticles with Mixed Ligands in Microphase Separated Block Copolymers. *Adv. Mater.* **2008**, *20*, 1462−1466.
(33) Mendoza, C.; Pietsch, T.; Gutmann, J. S.; Jehnichen, D.; Gindy, N.; Fahmi, A. Block Copolymers with Gold Nanoparticles: Correlation between Structural Characteristics and Mechanical Properties. *Macromolecules* **2009**, *42*, 1203−1211.
(34) Jang, S. G.; Khan, A.; Hawker, C. J.; Kramer, E. J. Morphology Evolution of PS-*b*-P2VP Diblock Copolymers via Supramolecular Assembly of Hydroxylated Gold Nanoparticles. *Macromolecules* **2012**, *45*, 1553−1561.
(35) Minelli, C.; Hinderling, C.; Heinzelmann, H.; Pugin, R.; Liley, M. Micrometer-Long Gold Nanowires Fabricated Using Block Copolymer Templates. *Langmuir* **2005**, *21*, 7080−7082.
(36) Chai, J.; Buriak, J. M. Using Cylindrical Domains of Block Copolymers To Self-Assemble and Align Metallic Nanowires. *ACS Nano* **2008**, *2*, 489−501.
(37) Zhang, X.; Qiao, Y.; Xu, L.; Buriak, J. M. Constructing Metal-Based Structures on Nanopatterned Etched Silicon. *ACS Nano* **2011**, *5*, 5015−5024.
(38) Pavan, M. J.; Shenhar, R. Two-Dimensional Nanoparticle Organization Using Block Copolymer Thin Films as Templates. *J. Mater. Chem.* **2011**, *21*, 2028−2040.
(39) Mezour, M. A.; Perepichka, I. I.; Zhu, J.; Lennox, R. B.; Perepichka, D. F. Directing the Assembly of Gold Nanoparticles with Two-Dimensional Molecular Networks. *ACS Nano* **2014**, *8*, 2214−2222.
(40) Kitching, H.; Shiers, M. J.; Kenyon, A. J.; Parkin, I. P. Self-Assembly of Metallic Nanoparticles into One Dimensional Arrays. *J. Mater. Chem. A* **2013**, *1*, 6985−6999.
(41) Matsushita, T.; Fukumoto, Y.; Kawakami, T.; Tsuruoka, T.; Murashima, T.; Yanagishita, T.; Masuda, H.; Nawafune, H.; Akamatsu, K. In Situ Template Synthesis of One-Dimensional Gold Nanoparticle Arrays in Organic Nanowires. *RSC Adv.* **2013**, *3*, 16243−16246.
(42) Jiang, L.; Sun, Y.; Nowak, C.; Kibrom, A.; Zou, C.; Ma, J.; Fuchs, H.; Li, S.; Chi, L.; Chen, X. Patterning of Plasmonic Nanoparticles into Multiplexed One-Dimensional Arrays Based on Spatially Modulated Electrostatic Potential. *ACS Nano* **2011**, *5*, 8288−8294.
(43) Lu, Q.; Bazuin, C. G. Solvent-Assisted Formation of Nanostrand Networks from Supramolecular Diblock Copolymer/Surfactant Complexes at the Air/Water Interface. *Nano Lett.* **2005**, *5*, 1309−1314.
(44) Perepichka, I. I.; Badia, A.; Bazuin, C. G. Nanostrand Formation of Block Copolymers at the Air/Water Interface. *ACS Nano* **2010**, *4*, 6825−6835.
(45) Perepichka, I. I.; Lu, Q.; Badia, A.; Bazuin, C. G. Understanding and Controlling Morphology Formation in Langmuir−Blodgett Block Copolymer Films Using PS-P4VP and PS-P4VP/PDP. *Langmuir* **2013**, *29*, 4502−4519.
(46) Zhu, J.; Eisenberg, A.; Lennox, R. B. Interfacial Behavior of Block Polyelectrolytes. 5. Effect of Varying Block Lengths on the Properties of Surface Micelles. *Macromolecules* **1992**, *25*, 6547−6555.
(47) Li, S.; Clarke, C. J.; Eisenberg, A.; Lennox, R. B. Langmuir Films of Polystyrene-*b*-Poly(alkyl acrylate) Diblock Copolymers. *Thin Solid Films* **1999**, *354*, 136−141.
(48) Devereaux, C. A.; Baker, S. M. Surface Features in Langmuir−Blodgett Monolayers of Predominantly Hydrophobic Poly(styrene)−Poly(ethylene oxide) Diblock Copolymer. *Macromolecules* **2002**, *35*, 1921−1927.
(49) Cheyne, R. B.; Moffitt, M. G. Novel Two-Dimensional "Ring and Chain" Morphologies in Langmuir−Blodgett Monolayers of PS-*b*-PEO Block Copolymers:Effect of Spreading Solution Concentration on Self-Assembly at the Air−Water Interface. *Langmuir* **2005**, *21*, 5453−5460.
(50) Cheyne, R. B.; Moffitt, M. G. Controllable Organization of Quantum Dots into Mesoscale Wires and Cables via Interfacial Block Copolymer Self-Assembly. *Macromolecules* **2007**, *40*, 2046−2057.
(51) Glagola, C. P.; Miceli, L. M.; Milchak, M. A.; Halle, E. H.; Logan, J. L. Polystyrene−Poly(ethylene oxide) Diblock Copolymer: The Effect of Polystyrene and Spreading Concentration at the Air/Water Interface. *Langmuir* **2012**, *28*, 5048−5058.
(52) Turkevich, J.; Stevenson, P. C.; Hillier, J. A Study of the Nucleation and Growth Processes in the Synthesis of Colloidal Gold. *Discuss. Faraday Soc.* **1951**, *11*, 55−75.
(53) Frens, G. Controlled Nucleation for the Regulation of the Particle Size in Monodisperse Gold Suspensions. *Nature Phys. Sci.* **1973**, *241*, 20−22.
(54) van Zoelen, W.; Alberda van Ekenstein, G.; Ikkala, O.; ten Brinke, G. Incorporation of PPE in Lamellar Self-Assembled PS-*b*-P4VP(PDP) Supramolecules and PS-*b*-P4VP Diblock Copolymers. *Macromolecules* **2006**, *39*, 6574−6579.
(55) van Zoelen, W.; Polushkin, E.; ten Brinke, G. Hierarchical Terrace Formation in PS-*b*-P4VP(PDP) Supramolecular Thin Films. *Macromolecules* **2008**, *41*, 8807−8814.
(56) Perepichka, I. I.; Borozenko, K.; Badia, A.; Bazuin, C. G. Pressure-Induced Order Transition in Nanodot-Forming Diblock Copolymers at the Air/Water Interface. *J. Am. Chem. Soc.* **2011**, *133*, 19702−19705.
(57) Antonietti, M.; Wenz, E.; Bronstein, L.; Seregina, M. Synthesis and Characterization of Noble Metal Colloids in Block Copolymer Micelles. *Adv. Mater.* **1995**, *7*, 1000−1005.
(58) Ono, L. K.; Cuenya, B. R. Formation and Thermal Stability of Au_2O_3 on Gold Nanoparticles: Size and Support Effects. *J. Phys. Chem. C* **2008**, *112*, 4676−4686.
(59) Yan, M.; Harnish, B. A Simple Method for the Attachment of Polymer Films on Solid Substrates. *Adv. Mater.* **2003**, *15*, 244−248.
(60) Harnish, B.; Robinson, J. T.; Pei, Z.; Ramström, O.; Yan, M. UV-Cross-Linked Poly(vinylpyridine) Thin Films as Reversibly Responsive Surfaces. *Chem. Mater.* **2005**, *17*, 4092−4096.
(61) Kim, K.; Ryoo, H.; Lee, Y. M.; Shin, K. S. Adsorption Characteristics of Au Nanoparticles onto Poly(4-vinylpyridine) Surface Revealed by QCM, AFM, UV/Vis, and Raman Scattering Spectroscopy. *J. Colloid Interface Sci.* **2010**, *342*, 479−484.
(62) Dong, H.; Fey, E.; Gandelman, A.; Jones, W. E., Jr. Synthesis and Assembly of Metal Nanoparticles on Electropun Poly(4-vinylpyridine) Fibers and Poly(4-vinylpyridine) Composite Fibers. *Chem. Mater.* **2006**, *18*, 2008−2011.
(63) Xu, H.; Hong, R.; Wang, X.; Arvizo, R.; You, C.; Samanta, B.; Patra, D.; Tuominen, M. T.; Rotello, V. M. Controlled Formation of Patterned Gold Films via Site-Selective Deposition of Nanoparticles onto Polymer-Templated Surfaces. *Adv. Mater.* **2007**, *19*, 1383−1386.